

Examining potential energy surface through Chebyshev shape parametrization

K. Jyothish*, M. S. Suryan Sivadas,[†] and A. K. Rhine Kumar[‡]

Department of Physics, Cochin University of Science and Technology, Kochi-682022, India.

(Dated: August 11, 2025)

The present study introduces a novel approach, the Chebyshev shape parametrization, to describe the geometric configurations of atomic nuclei, with a particular emphasis on fission dynamics. In this framework, the nuclear surface is represented by a profile function expanded in a Chebyshev polynomial series, with deformation parameters derived analytically under volume conservation and centre-of-mass constraints. The proposed parametrization is shown to be universal robust, and we establish transformation equations that connect it to other widely used shape parametrizations. In the macroscopic approach, the potential energy surface (PES) is computed using the Lublin–Strasbourg Drop (LSD) model, incorporating deformation-dependent energy coefficients expressed in terms of Chebyshev parameters. This enables a detailed investigation of the structural evolution and fission pathways of the nucleus ^{227}Pa across various deformations, depicting the influence of shape parameters on elongation, asymmetry, and neck formation. Complementing this, microscopic analysis is carried out by calculating single-particle energy levels through diagonalization of the Yukawa-folded mean-field Hamiltonian in a deformed harmonic oscillator basis. The nuclear shape parameters are provided by the Chebyshev parametrization, allowing us to examine shell structure effects at specific deformations. Together, these macroscopic and microscopic studies provide comprehensive insight into the nuclear energy landscape and shape evolution during fission.

I. INTRODUCTION

In recent years, significant theoretical developments have been made in the dynamic reshaping of atomic nucleus during the fission process [1–3]. However, a comprehensive theoretical framework that explains the complexities of fission reactions continues to be challenging. The structural and dynamic evaluation of fission requires three essential components: nuclear shape parameterization, the total potential energy of the nucleus in terms of its deformation, and the differential equation describing its time evolution [4]. The primary objective is to select an appropriate shape parameterization or profile function to determine the shape of the nucleus [5, 6]. This function must converge rapidly with a minimal number of parameters to ensure simplicity and accuracy. It should be sufficiently flexible to represent a broad range of nuclear shapes, from spherical to highly distorted configurations, including dumbbell structures. Furthermore, the function must be compatible with current theoretical models and ensure computational efficiency. Various shape parametrization methods have been incorporated into theoretical models to explore the potential energy landscape of atomic nuclei [7–9]. Among these methods include Bohr-Mottelson shape parametrization (β, γ) [10], Cassini ovals [11, 12], quadratic surfaces of revolution (QSR) [13, 14], Funny-Hills (F-H) shapes [15–17], modified Funny-Hills [18], Trentalange-Koonin-Sierk (TKS) shape parametrization [19], and Fourier shape parametrization [20]. Still the scientific communities are exploring new parametrization methods to investigate all

the changes during the fission. The present work proposes a new, rapidly converging shape parametrization, the Chebyshev shape parametrization, to describe all the possible geometric configurations of the atomic nucleus. The second key objective is to evaluate the total potential energy of the nucleus. Nuclear theoretical frameworks to unveil the potential energy landscapes are categorized into different paradigms. The first encompasses the microscopic approach, including the relativistic mean field model [21, 22], Hartree-Fock-Bogoliubov with Skyrme [23, 24] or Gony forces [25], quantum field theory [22], and density functional theories [26]. The second category includes phenomenological macroscopic models developed following George Gamow’s liquid drop model (LDM) [27–29], such as the droplet model (DM), the finite-range droplet model (FRDM) [30], and the Lublin-Strasbourg drop (LSD) model [31]. LSD model relatively modernized LDM by incorporating the curvature and congruence terms expressed through Leptodermous expansion. By the 1970s, it became clear that the LDM was inadequate for replicating measured fission barrier heights. This realization led to the development of extensions to LDM with microscopic contributions as proposed by Strutinsky [32, 33]. The macroscopic-microscopic methods calculate the potential energy as the sum of shape-dependent macroscopic and microscopic terms. These shape-dependent terms make them computationally efficient, allowing for rapid predictions within a multidimensional deformation space across the nuclear landscape [31, 34–37]. The macroscopic-microscopic method is notable for its effectiveness in explaining various aspects of atomic nuclei, including shape coexistence [34, 38], hyperdeformation [39], stability of super heavy nuclei [40], and giant dipole resonances [41]. However, as temperature increases, the microscopic contribution diminishes, leaving the macroscopic contribution domi-

* jyothishk003@gmail.com, jyothishk003@cusat.ac.in

[†] ms3.mssivadas@cusat.ac.in

[‡] rhinekumar@cusat.ac.in

nant [6].

In the present scenario exploring a new shape parametrization to define the nuclear geometry and study the resulting changes in the potential energy has relevance. We define the nuclear geometry using Chebyshev shape parametrization and the deformation induced changes in the potential energy are explained by exerting the LSD model.

Sec. II presents the theoretical framework, divided into three subsections. Sec. II A details the proposed profile function for nuclear geometry and the essential quantities for formulating various nuclear shapes. Sec. II B establishes the relationship between Chebyshev shape parametrization and other existing parametrization techniques. Sec. II C discusses the model used to determine the total potential energy. The results are presented in Sec. III, where a detailed study of the potential energy surface as a function of different deformation parameters is conducted. The conclusions are detailed in Sec. IV.

II. THEORETICAL FRAMEWORK

A. Chebyshev shape parametrization

Chebyshev polynomials play a significant role in numerical analysis and approximation theories, providing advantages over the Power, Legendre, and Fourier series. The orthogonality of Chebyshev polynomials minimizes round-off error accumulation, addressing the numerical instability often associated with the power series [42]. With nodes clustered at the boundaries, Chebyshev interpolation reduces Runge's phenomenon and offers better accuracy than evenly spaced nodes in power series. In contrast, Legendre nodes, denser at the centre, tend to amplify it [43]. Unlike the Fourier series, which is optimized for periodic functions, Chebyshev polynomials are naturally suited for bounded and non-periodic domains $[-1,1]$, making them ideal for modelling irregular geometrical shapes and solving boundary-value problems. Moreover, they are less prone to the Gibbs phenomenon, offering improved accuracy for sharp transitions and boundary-layer effects [44]. The exponential convergence of the Chebyshev series for analytic functions within the ellipse of convergence surpasses that of the Legendre and the power series [45]. They are particularly valued for their minimax property, which minimizes the maximum error in polynomial approximations [46]. Efficient evaluation algorithms, such as the Clenshaw algorithm [47], make the computation of Chebyshev polynomials straightforward and fast. This computational efficiency is advantageous in real-time applications and in large-scale numerical simulations.

We developed a shape parametrization method using Chebyshev polynomials of the first kind ($T_n(x)$), addressing the limitations of existing parametrization methods. They excel in representing non-periodic phenomena within confined spaces, making them particularly useful

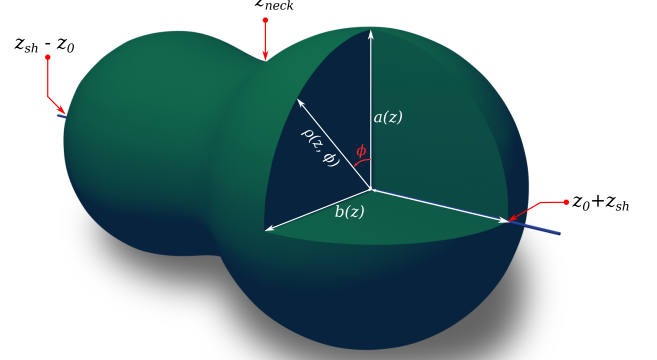


FIG. 1. Schematic representation of the geometry of nucleus in cylindrical coordinates using the Chebyshev profile function.

for understanding the potential energy landscape of the atomic nuclei. Nuclear shape parametrization as a profile function using Chebyshev series expansion in a cylindrical coordinate (r, ϕ, z) system is written as,

$$\frac{\rho_s^2(u)}{R_0^2} = \sum_{n=0}^{\infty} a_n T_n(u), \quad (1)$$

$$T_n(u) = \cos[n \cos^{-1}(u)] \quad \text{if} \quad -1 \leq u \leq 1.$$

$\rho_s(u)$ represents the perpendicular distance from a surface point to the symmetry axis (z axis), where $u = \frac{z - z_{sh}}{z_0}$, R_0 denotes the radius of a spherical shape with the same volume as the nuclear shape being considered. a_n is the Chebyshev series coefficient, which is considered the deformation parameter for explaining different shapes of the nucleus. Along the symmetry axis, the shape extends by a length of $2z_0$, with its left and right ends positioned at $z_{\min} = z_{sh} - z_0$ and $z_{\max} = z_{sh} + z_0$, respectively. z_{sh} is the shift coordinate, which will be discussed in the section II A 2. The boundary condition of the profile function can be written as, $\rho_s^2(z_{\min}) = \rho_s^2(z_{\max}) = 0$, which gives the following relation,

$$\begin{aligned} \sum_{n=0}^{\infty} a_n T_n(-1) &= \sum_{n=0}^{\infty} (-1)^n a_n = 0, \\ \sum_{n=0}^{\infty} a_n T_n(1) &= \sum_{n=0}^{\infty} a_n = 0. \end{aligned} \quad (2)$$

a_0 and a_1 are estimated from the above conditions,

$$a_0 = - \sum_{n=2,4,\dots}^{\infty} a_n, \quad a_1 = - \sum_{n=3,5,\dots}^{\infty} a_n. \quad (3)$$

1. Volume conservation

The nucleus is treated as an incompressible liquid drop with a constant volume. Thus, the volume equivalence between a sphere and a deformed nucleus can be stated as,

$$V = \frac{4\pi}{3}R_0^3 = \int_0^{2\pi} d\phi \int_{z_{\min}}^{z_{\max}} dz \int_0^{\rho_s(z)} \rho d\rho, \quad (4)$$

$$= \pi \int_{z_{\min}}^{z_{\max}} \rho_s^2(z) dz.$$

The length of the nucleus in terms of elongation (c) is defined as $z_0 = cR_0$, which can be obtained by simplifying Eq. 4 and relationship between c and all even coefficients, a_{2n} is formulated as,

$$\sum_{n=0}^{\infty} \frac{a_{2n}}{1 - 4n^2} = \frac{2}{3c}. \quad (5)$$

Eq. 5 is analogous to the volume conservation relation in the Funny-Hills (F-H) parameterization and the Fourier shape parametrization [48–51]. This volume conservation equation can find a_2 and its higher order as a function of elongation (c). The nucleus adopt a spherical shape when c equals one, however, if c decreases or increases from this value, the nucleus exhibits either an oblate or prolate shape, respectively. Considering the nucleus in a spheroidal condition by limiting Eq. 5 to $n = 1$, we can obtain the relation $c = -1/2a_2$. The spherical, prolate and oblate nuclear shapes can be obtained by the conditions $a_2 = -\frac{1}{2}$, $-\frac{1}{2} < a_2 < 0$ and $a_2 < -\frac{1}{2}$ respectively, where a_2 is the sole shape-determining parameter. For higher values of n , additional shape-determining parameters emerge, potentially leading to the breakdown of the simple spheroidal condition and the formation of more complex structures, such as a dumbbell shape.

2. Centre of mass formalism

Given the inherent asymmetry in the shape of the system, fixing the system's centre of mass becomes necessary. The general equation with respect to the z -axis can be described mathematically as [20],

$$z_{cm} = \frac{\int_v z \rho d^3r}{\int_v \rho d^3r} = \frac{\pi \int_{z_{\min}}^{z_{\max}} \rho_s^2(z) z dz}{\pi \int_{z_{\min}}^{z_{\max}} \rho_s^2(z) dz} = 0. \quad (6)$$

To address the geometry of the left-right asymmetry in the nucleus during the fission process, a new term was introduced, named as shift coordinate (z_{sh}), which ensures that the center of mass of the nucleus is positioned at the origin. This quantity is zero when all the odd deformation parameters a_n are equal to zero. This shift coordinate is derived from the Eq. 6 and expressed as,

$$z_{sh} = \frac{3cz_0}{2} \sum_n \frac{a_{2n+1}}{(2n+1)^2 - 4}. \quad (7)$$

3. Distance between nascent fragments

Determining the distance between the centre of mass of the nascent left-right fragments (R_{12}) is essential for fission studies, which can be obtained as,

$$R_{12} = \frac{\pi \int_{z_{\text{neck}}}^{z_{\max}} \rho_s^2(z) z dz}{\pi \int_{z_{\text{neck}}}^{z_{\max}} \rho_s^2(z) dz} - \frac{\pi \int_{z_{\min}}^{z_{\text{neck}}} \rho_s^2(z) z dz}{\pi \int_{z_{\min}}^{z_{\text{neck}}} \rho_s^2(z) dz}. \quad (8)$$

Here, z_{neck} represents the position at which the fission fragments are formed. At this point, the function ρ_s reaches its minimum, and the nucleus approaches the scission point, corresponding to $\frac{d\rho_s}{dz} = 0$. To facilitate the analysis, a new coordinate u_{neck} can be introduced, which is defined as $u_{\text{neck}} = \frac{(z_{\text{neck}} - z_{sh})}{z_0}$. From the minimization condition, a relation can be obtained as,

$$R_{12} = \frac{\sum_{m=0}^{\infty} (-1)^m a_{2m+1} (2m+1)}{\sum_{m=0}^{\infty} (-1)^m a_{2m} 4m^2}, \quad (9)$$

by retaining terms only up to a_4 in the summation, the neck thickness can be approximated as,

$$R_{12} = \frac{a_3}{a_2 - 4a_4}. \quad (10)$$

4. Realistic profile function: Non-axial case

Since the nucleus' deformation might not be strictly axial, we have included a non-axial parameter to better capture its true structure. Consider the equation of ellipsoid, which depends on the deformation of nucleus [52],

$$\frac{x^2}{a_x^2} + \frac{y^2}{a_y^2} = 1, \quad (11)$$

where a_x and a_y are half-axis parameters. The equation of ellipsoid in polar coordinates is written as,

$$\rho^2(z, \phi) = \frac{a_x^2 a_y^2}{a_y^2 \cos^2(\phi) + a_x^2 \sin^2(\phi)}, \quad (12)$$

The non-axiality parameter η is the relative difference of the half axis of the cross-section perpendicular to the symmetry axis and is given by [40],

$$\eta = \frac{a_y - a_x}{a_y + a_x}. \quad (13)$$

It describes the extent of non-axiality occurs due to the deformation of nucleus. For an axially symmetric shape, η becomes zero. Here, we consider the volume of the deformed nucleus to be the same as that of the spherical nucleus. Hence, the volume conservation equation becomes,

$$\pi \rho^2 = \pi a_x a_y. \quad (14)$$

For the pure ellipsoidal shape, the half axis can be described in terms of deformation parameters c and η as follows,

$$a_x = \frac{R_0}{\sqrt{c}} \left(\frac{1-\eta}{1+\eta} \right)^{1/2}, a_y = \frac{R_0}{\sqrt{c}} \left(\frac{1+\eta}{1-\eta} \right)^{1/2}, a_z = R_0 c. \quad (15)$$

A non-axial nuclear shape can be derived by incorporating the η parameter into the axial-profile function ($\rho_s(z, \phi)$). This approach leads to a more realistic representation of the nuclear profile function, which is expressed as,

$$\rho^2(z, \phi) = \rho_s^2(z) \frac{1-\eta^2}{1+\eta^2+2\eta\cos(2\phi)}. \quad (16)$$

A schematic diagram depicting an elongated, dumbbell shaped, axially symmetric nuclear surface along the z -axis is illustrated in Fig. 1.

5. Convergence properties

A key advantage of using the Chebyshev parametrization, as shown in Eq. 1, is its flexibility in precision. This approach can be extended to any desired order, allowing for a detailed study of its convergence properties.

Fig. 2 compares the convergence of Chebyshev and Fourier shape parametrizations for a specific nuclear shape through the profile function and its coefficients. The figure consists of seven subplots: the nuclear profile function $\rho^2(u)$, $\rho(u)$, and the contributions from different orders of expansion to the shape function, specifically, a_2, a_3, a_4, a_5 and a_6 as functions of u . Chebyshev coefficients exhibit faster convergence across orders than Fourier coefficients, indicating greater efficiency in accurately representing nuclear surface deformations. The figure also shows that the contributions of a_5 and a_6 are almost negligible in Chebyshev shape parametrization compared to Fourier shape parametrization, further supporting its efficiency.

The a_2 component has a value of 0.2, while a_6 drops to approximately 0.01, over an order of magnitude lower. Similarly, a_5 , at 0.02, is also more than an order of magnitude smaller than a_3 which is approximately 0.3. This pattern illustrates how higher order terms contribute minimally, enabling precise control over shape details with only a few leading terms. The lowest-order term, a_2 primarily controls the elongation of shape, while the next term, a_3 introduces left-right asymmetry a_4 defines the neck formation and a_5 adds only minor distortions in left-right asymmetry. The parameter a_6 further refines the neck with minimal adjustment. Generally, higher-order Chebyshev coefficients (both even and odd) have a small or negligible impact on the shape. To determine the potential energy surface, we utilized three Chebyshev parameters a_2, a_3 and a_4 along with an additional non-axiality parameter, η .

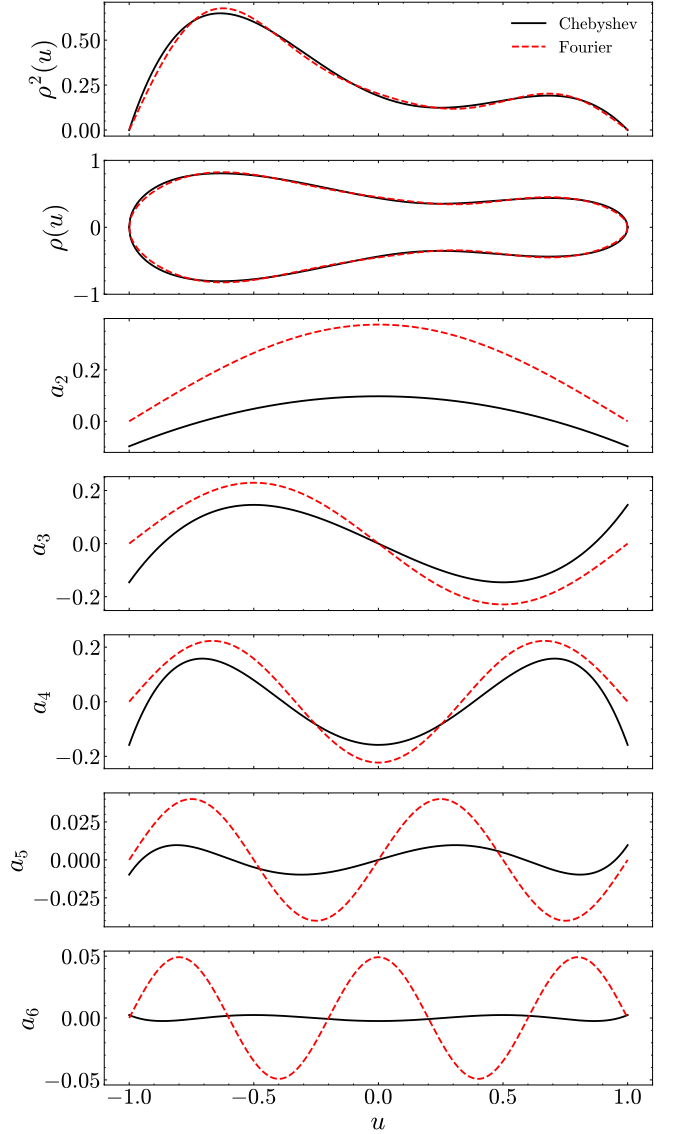


FIG. 2. Comparison of the convergence between Chebyshev and Fourier shape parametrizations for a specific nuclear shape, depicted through subplots of the profile functions $\rho^2(u)$ and $\rho(u)$, alongside contributions from different orders of expansion (a_2 to a_6) as functions of u .

Using Eq. 1, a series of nuclear shapes characterized by deformation parameters a_2, a_3 , and a_4 have been plotted and are shown in Fig. 2. In the first row, a_3 and a_4 are fixed, and a_2 is varied, generating spherical, prolate, and oblate shapes. It demonstrates that a_2 characterizes the elongation of the nucleus. In the second row, a_2 and a_3 are fixed and a_4 is varied. By fixing $a_3 = 0$, we got a symmetric dumbbell shape. By gradually increasing the negative value of a_4 , the relative neck thickness of the shapes increases, indicating that a_4 controls the neck formation. In the third row, a_2 and a_4 are fixed, while a_3 is varied. This results in left and right asymmetric shapes for $a_3 = 0.5$ and -0.5 , respectively, with a mod-

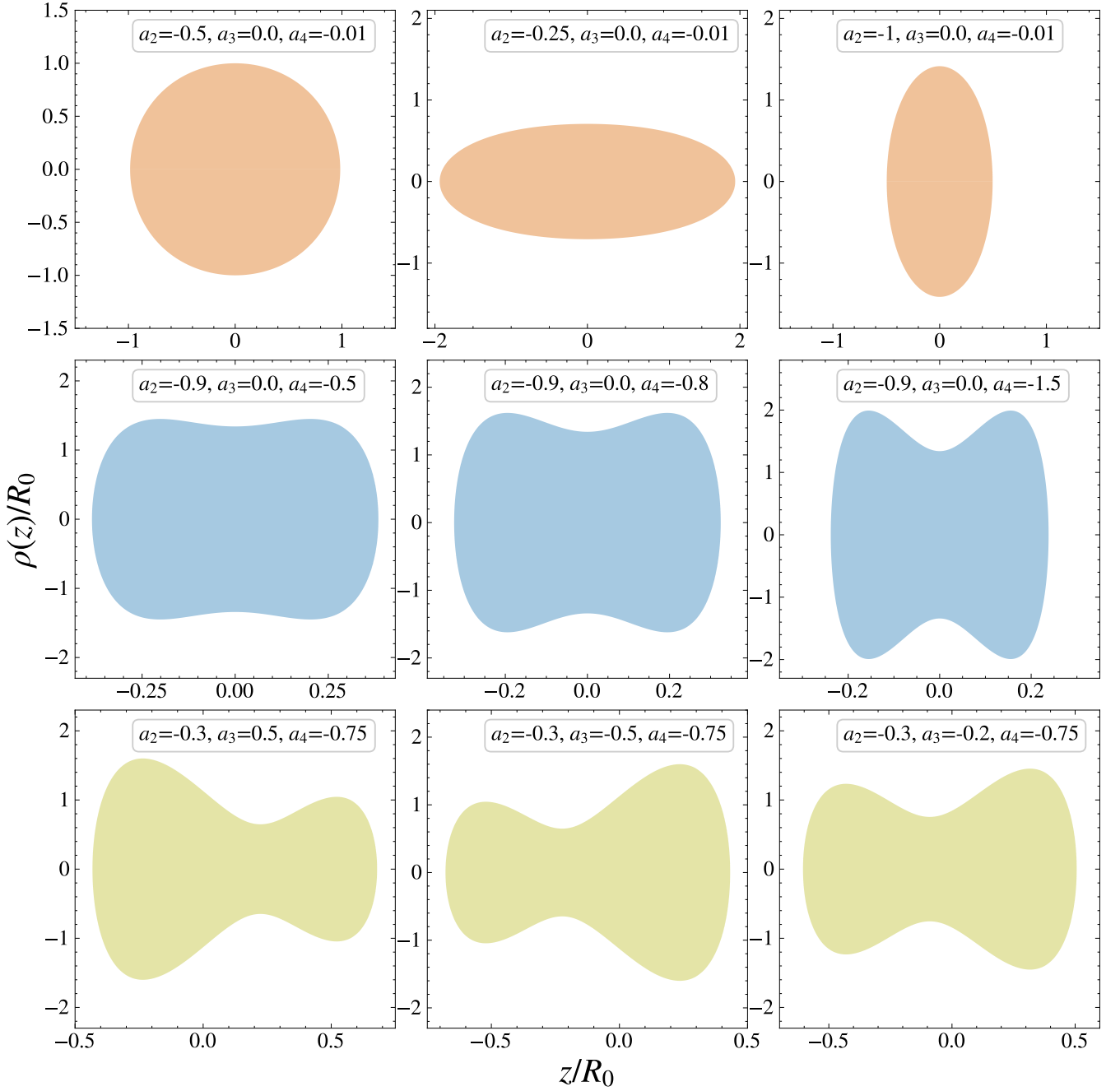


FIG. 3. Possible nuclear shapes using Chebyshev shape parametrization with different deformation parameters.

erately asymmetric shape plotted for $a_3 = -0.2$. Therefore, the odd parameters of the Chebyshev polynomials characterize the asymmetric shape of the nucleus, and the even parameters control the relative elongation and neck formation of the nucleus. Hence, the Chebyshev shape parametrization effectively captures the diverse shapes during fission.

B. Relation with other shape parametrization

1. Bohr-Mottelson shape parametrization (β, γ)

Bohr-Mottelson shape parametrization (β, γ) , is suitable for minor to moderate deformations, and becomes complex for highly deformed structures with substantial number of terms up to β_{14} to accurately represent nuclear shapes and their liquid-drop energy during the fission process [53–55]. Furthermore, the function does not

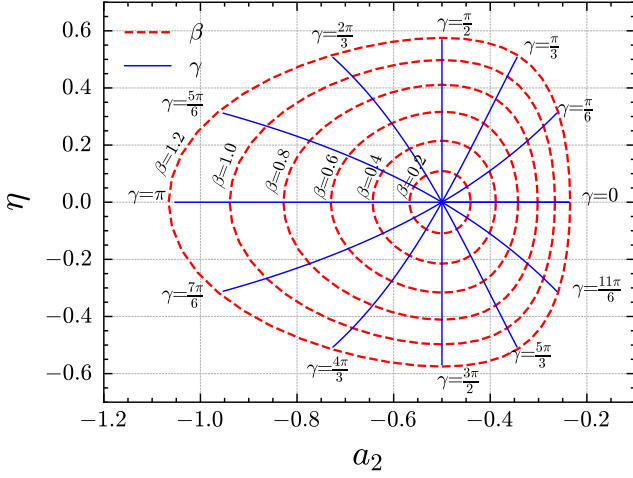


FIG. 4. The relationship between traditional Bohr-Mottelson shape parameters (β, γ) and Chebyshev parameters (a_2, η) .

converge rapidly when a nucleus is highly elongated, particularly between the saddle and scission points [18]. The relationship between generally used (β, γ) and the (η, c) can be derived from the half-axis formula of the ellipsoid [56]. The half-axis formula in terms β and γ is defined as [40],

$$\begin{aligned} R_x &= R_0 \exp \left(\sqrt{\frac{5}{4\pi}} \beta \cos(\gamma - 2\pi/3) \right) = \frac{R_0}{\sqrt{c}} \left(\frac{1-\eta}{1+\eta} \right)^{1/2} \\ R_y &= R_0 \exp \left(\sqrt{\frac{5}{4\pi}} \beta \cos(\gamma - 4\pi/3) \right) = \frac{R_0}{\sqrt{c}} \left(\frac{1+\eta}{1-\eta} \right)^{1/2} \\ R_z &= R_0 \exp \left(\sqrt{\frac{5}{4\pi}} \beta \cos \gamma \right) = R_0 c \end{aligned}$$

Using the above equations, we can establish the relationship between (β, γ) and (η, a_2) .

$$\beta = \left\{ \frac{4\pi}{5} \left[\frac{1}{3} \log^2 \left(\frac{1+\eta}{1-\eta} \right) + \log^2 \left(-\frac{1}{2a_2} \right) \right] \right\}^{1/2} \quad (17)$$

$$\gamma = \tan^{-1} \left[\frac{1}{\sqrt{3}} \frac{\log \left(\frac{1+\eta}{1-\eta} \right)}{\log \left(-\frac{1}{2a_2} \right)} \right] \quad (18)$$

Fig. 4 illustrates the relationship between (β, γ) and (a_2, η) , obtained from Eqs. 17 and 18 respectively. This relationship holds only under spheroidal deformation, and breaks down if the system adopts a dumbbell shape. The figure demonstrates a 60° symmetry, indicating that the exact shape repeats every 60° . For example, consider an axially symmetric prolate shape at deformation parameters $(\beta = 0.1, \gamma = 0^\circ)$ with $(a_2 \approx -0.47, \eta = 0)$. This shape is identical to the one at $(\beta = 0.1, \gamma = 120^\circ)$

with $(a_2 \approx -0.52, \eta \approx 0.06)$. Similarly, an axially symmetric oblate shape at $(\beta = 0.6, \gamma = 180^\circ)$ with $(a_2 \approx -0.73, \eta = 0)$ is equivalent to the shape at $(\beta = 0.6, \gamma = 60^\circ)$ with $(a_2 \approx -0.42, \eta \approx 0.28)$. These equivalences occur for spheroidal shapes when higher-order Chebyshev shape parameters (a_n for $n > 2$) are neglected. It is observed that a larger value of β can't be attributed to the elongation of shape, and a non-axial parameter, η , will have a finite value as illustrated in Fig. 4. This observation indicates the (a_2, η) deformation space is more appropriate for exploring the triaxial shapes than the conventional (β, γ) space. Hence, Chebyshev shape parametrization offers a more comprehensive framework for describing the shape of nucleus.

2. Funny-Hills shape parametrization

F-H shape parametrization introduces additional solutions between the boundary conditions for certain combinations of deformation parameters, which leads to negative values of $\rho_s^2(z)$. This illogical and unphysical outcome necessitates the modifications to this parametrization. Although the modified F-H parametrization provides valuable insights into the fission barrier, it often struggles to accurately predict the energies of fissioning nucleus, with limited improvements achievable by adjusting the deformation parameters [57].

The F-H shape parametrization for $B \geq 0$ can be regarded as a special case of the Chebyshev shape parametrization. The relationship between these two parametrizations can be established by comparing the coefficients of their respective variables.

$$\begin{aligned} a_2 &= -\frac{c^2 A}{2} \\ a_3 &= -\frac{c^2 \alpha}{4} \\ a_4 &= -\frac{c^2 B}{8} \end{aligned} \quad (19)$$

Where, A, B , and α are the F-H deformation parameters and c is the common elongation parameter.

3. TKS shape parametrization

The precision of TKS parametrization based on the Legendre polynomial approach can be improved by the higher-order expansions. However, it is constrained by the requirement of $\rho_s^2(z) \geq 0$, which limits the number of deformation parameters.

Similarly, a transformation relation between the Chebyshev and TKS shape variables (a_2, a_3, a_4) can be formulated and approximated up to the fourth degree as

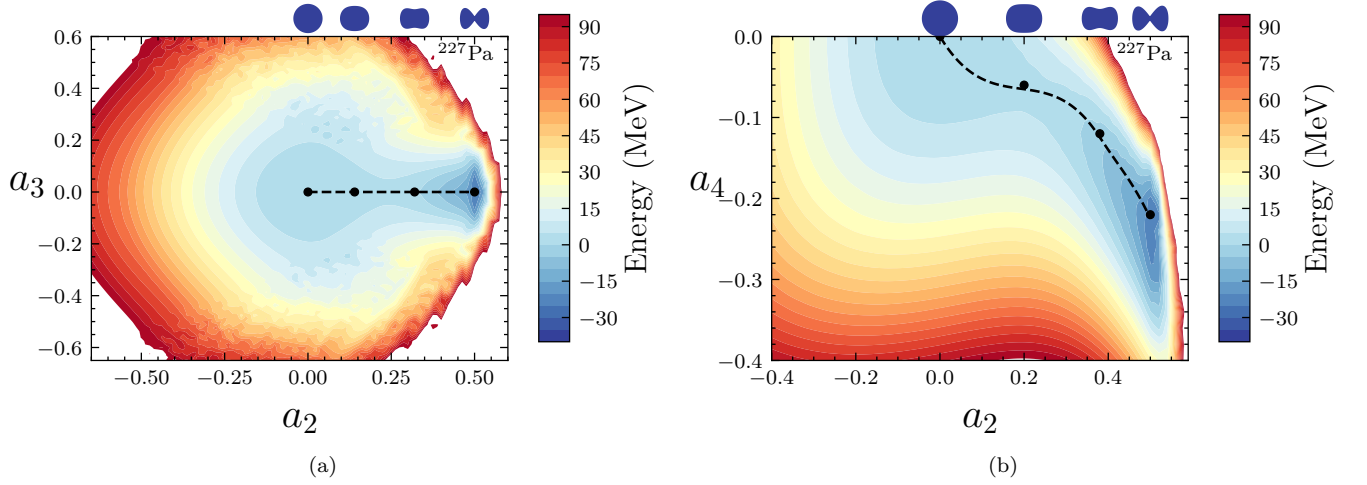


FIG. 5. Cross sections of PES of ^{227}Pa at $L = 0$ in the two-dimensional deformation subspace defined by (a) (a_2, a_3) , and (b) (a_2, a_4) , remaining parameters are fixed at values corresponding to the minimum potential energy of the fissioning nucleus.

given below,

$$\begin{aligned} a_2 &= \frac{3}{4}\alpha_2 - \frac{5}{16}\alpha_4 \\ a_3 &= \frac{5}{8}\alpha_3 \\ a_4 &= \frac{105}{192}\alpha_4. \end{aligned} \quad (20)$$

4. Fourier shape parametrization

The Fourier shape parametrization has recently emerged as a promising alternative, facilitating rapid convergence properties that provide crucial information about the fission process near the scission point. It offers detailed descriptions of highly elongated and necked nuclear shapes utilizing only a few deformation parameters. [58, 59, 61, 62]. The evaluation of the relation between Coefficients of Fourier shape parametrization and Chebyshev shape parametrization is as follows,

$$\begin{aligned} a_0 &= \sum_{n=1}^{\infty} f_{2n} J_0 \left(\frac{(2n-1)\pi}{2} \right) \\ a_1 &= 2 \sum_{n=1}^{\infty} f_{2n+1} J_1 \left(\frac{2n\pi}{2} \right) \\ a_{2m} &= \sum_{m=1}^{\infty} \left[2(-1)^m \sum_{n=1}^{\infty} f_{2n} J_{2m} \left(\frac{(2n-1)\pi}{2} \right) \right] \\ a_{2m+1} &= \sum_{m=1}^{\infty} \left[2(-1)^m \sum_{n=1}^{\infty} f_{2n+1} J_{2m+1} \left(\frac{2n\pi}{2} \right) \right] \end{aligned} \quad (21)$$

where J_n is the n^{th} -order Bessel function of first kind, and f_n represents the Fourier shape parameters. Therefore, we successfully demonstrated that the Chebyshev shape

parametrization is more universal, consistent, and robust since it can establish a significant relationship between all the existing shape parametrizations.

C. Potential energy calculation

Following the determination of the nuclear geometry, the next phase entails a comprehensive characterization of the system's potential energy throughout the fission process. The energy of the nucleus is computed via two complementary frameworks, the macroscopic and microscopic approaches. Each employs Chebyshev shape parametrization to compute the nuclear potential energy for different deformation parameters.

1. Macroscopic approach

To calculate the macroscopic energy, the Lublin-Strasbourg Drop (LSD) model is employed among the various liquid drop formulations. Unlike the traditional Liquid Drop Model (LDM), the LSD model includes additional energy contributions such as curvature and congruence terms, allowing for a more refined evaluation of the macroscopic potential energy of the system. The potential energy terms can be expressed as a leptodermous expansion with respect to the atomic

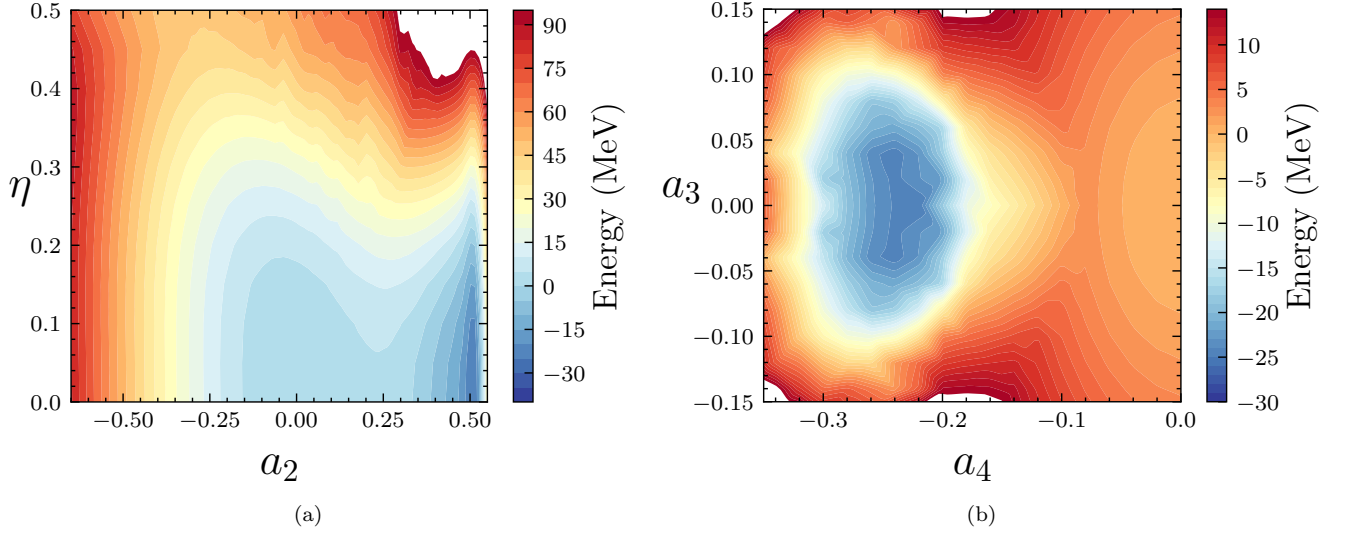


FIG. 6. Similar to Fig. 5, but for the deformation subspace defined by (a) (a_2, η) , and (b) (a_4, a_3) .

mass, formulated as follows [31],

$$\begin{aligned}
 V(a_i)_{\text{LSD}} = & b_{\text{surf}}(1 - k_{\text{surf}}I^2)(B_s(a_i) - 1) \\
 & + \frac{3}{5} \frac{e^2 Z^2}{r_0 A^{1/3}} (B_C(a_i) - 1) \\
 & + E_r^{(0)}(L^2 B_j(a_i) + K^2 B_k(a_i)) \\
 & + b_{\text{curv}}(1 - k_{\text{curv}}I^2)(B_{\text{curv}}(a_i) - 1) \\
 & + E_{\text{cong}}^{(0)}(B_{\text{cong}}(a_i) - 1).
 \end{aligned} \quad (22)$$

The rotational terms are incorporated following the approaches in refs.[16, 48]. $E_r^{(0)} = \frac{\hbar^2}{2J_0}$ is the rotational energy coefficient, where J_0 is the moment of inertia of the rigid sphere and L and K are the angular momenta with respect to the axis perpendicular and parallel to the symmetry axis, respectively. The deformation of the nucleus is denoted by the parameter a_i where $I = (N - Z)/A$ represents the reduced isospin. $B_s, B_C, B_{\text{curv}}, B_{\text{cong}}, B_j$ and B_k are the deformation-dependent coefficients associated with the surface, Coulombic, curvature, and rotational contributions, respectively, derived using Chebyshev shape parametrization. Additional constant parameters commonly used in LSD models are provided in Table I.

The deformation-dependent terms such as curvature and congruence energy terms play a pivotal role in the fission process. While the surface and curvature terms demonstrate similar behavior at small to moderate deformations. It is observed that the curvature term will dominate significantly as the deformation increases. Understanding this behavior is essential for improving the accuracy of models in predicting the nuclear binding energies and fission barriers. As the nucleus elongates and forms a neck, the congruence energy term (B_{cong}) dominates, which leads to the fission process. The equation

TABLE I. Parameters used in LSD model

$b_{\text{surf}} = 16.9707 \text{ MeV}$	$k_{\text{surf}} = 2.2938$
$b_{\text{curv}} = 3.8602 \text{ MeV}$	$k_{\text{curv}} = -2.3764$
$r_0 = 1.21725 \text{ fm}$	

used to determine the congruence energy is,

$$E_{\text{cong}}(a_i) = E_{\text{cong}}^{(0)}(I)B_{\text{cong}}(a_i) \quad (23)$$

$$B_{\text{cong}}(a_i) = \begin{cases} 2 - \frac{R_{\text{neck}}(a_i)}{R_{\text{frag}}(a_i)}, & \text{for necked-in shapes} \\ 1, & \text{otherwise} \end{cases}$$

$$E_{\text{cong}}^{(0)}(I) = -C_3 \exp(-W_2|I|C_3)$$

where $C_3 = 10 \text{ MeV}$ and $W_2 = 42 \text{ MeV}$. The strength of the neck formation depends on the radius of the neck ($R_{\text{neck}}(a_i)$) and the radius of the nascent light fission fragment ($R_{\text{frag}}(a_i)$), which in turn influences the deformation energy of the fissioning nucleus.

2. Microscopic approach

To complement the macroscopic modelling of the nuclear potential energy, a microscopic description is employed to evaluate the behaviour of individual nucleons in a deformed mean-field potential. This approach provides a more detailed understanding of how the single-particle energy levels evolve with nuclear deformation. In the present work, the microscopic structure is computed by solving the single-particle Schrödinger equation with a deformation-dependent mean-field Hamiltonian constructed using a finite-range Yukawa folding method [60].

The total single-particle Hamiltonian takes the form,

$$H = \frac{p^2}{2m} + V_N + V_C + V_{S-O} \quad (24)$$

The terms represent the kinetic energy, mean-field nuclear potential, Coulomb interaction, and spin-orbit coupling, respectively. As the nuclear surface is not sharply defined but exhibits a gradual fall-off in nucleon density, the nuclear, Coulomb, and spin-orbit potentials are all generated from a smooth, diffuse nucleon density distribution. This gradual decrease in density near the nuclear surface is known as surface diffuseness. The density profile, which captures the transition from the dense nuclear interior to the low-density surface region, is through a folding procedure using a finite-range interaction. The folded density is expressed as,

$$\rho(\vec{r}) = \rho_0 \int d^3r' g(|\vec{r} - \vec{r}'|) \quad (25)$$

where ρ_0 is the constant volume density and $g(|\vec{r} - \vec{r}'|)$ is a Yukawa-folding function with a realistic surface diffuseness.

$$|\vec{r} - \vec{r}'| = \sqrt{\rho^2 + \rho'^2 - 2\rho\rho' \cos(\phi - \phi') + (z - z')^2} \quad (26)$$

where, ρ , and ρ' are radial coordinates in cylindrical coordinate system. These coordinates are determined by the Chebyshev shape parametrization as shown in Eq. 1, which defines the nuclear surface and allows for the exploration of various deformation configurations. Consequently, the resulting V_N , V_C and V_{S-O} become functions of the nuclear shape, directly influencing the single-particle energy levels across different deformations.

III. RESULTS AND DISCUSSION

In the present study, we focused on the structural changes of ^{227}Pa nucleus during the fission process. This is facilitated by explaining the potential energy surface (PES), depicted using the newly introduced Chebyshev shape parametrization within the macroscopic approach based on LSD model. Recently, the different fission modes of the ^{227}Pa nucleus have been studied, confirming the presence of both symmetric and asymmetric fission modes[63, 64]. In our study, we carefully illustrate the PES for various combinations of deformation parameters, specifically (a_2, a_3) , (a_2, a_4) and (a_2, η) . While other parameters are fixed at values corresponding to the minimum potential energy of the fissioning nucleus at angular momentum $L=0$. The deformation parameters a_2 and a_4 are interconnected, such that a_2 primarily influences the elongation and a_4 affects the neck formation. The parameters a_3 and η represents asymmetry and non-axiality in the nuclear shape respectively.

Fig. 5(a) and (b) illustrates the PES within the two-dimensional deformation subspace defined by (a_2, a_3) and

(a_2, a_4) respectively. The remaining parameters are fixed at values corresponding to the minimum potential energy of the fissioning nucleus. The probable shape transitions from spherical to an extreme dumbbell shapes in the fission paths are depicted in the upper panel. In Fig. 5(a), the dashed line represents the most probable fission trajectory at $a_3 = 0$, which implies a symmetric fission path. At $a_2 = 0$, the nuclear shape is spherical, and further increase in a_2 causes an elongation of the nucleus and transforms to an ellipsoid followed by a symmetric dumbbell configuration at $a_2 = 0.5$. Along this path, the nucleus experiences a single-hump in the potential energy curve. Other minimum energy points corresponding to a_3 values from 0 to ± 0.1 , indicates that the left and right asymmetric fission can occur for the ^{227}Pa nucleus. The Fig. 5(b) reveals a minimum potential energy path to fission starts from (0,0) and reaches the scission point at (0.5, -0.26). The scission point spanned over a region of $a_4 = -0.2$ to -0.28 with $a_2 = 0.5$, indicating the possibility of a broader range of symmetric and asymmetric fission modes. As a_4 increases, the curvature and congruence effects influence the total potential energy, which alter the shape and gradually leading to the fission.

Fig. 6(a) and (b) illustrates the PES defined by (a_2, η) and (a_4, a_3) respectively. The nuclear shape at the ground state ($a_2 = 0$) is deformed to some degree than perfectly spherical. In Fig. 6(b) the first minimum potential energy point is at (0,0) and a minimum energy pathway leading to the fission is observed. This path is characterized by a_4 values ranging from 0 to -0.25 , with a saddle point at $(-0.08, 0)$. A second potential minimum is identified, extending from $a_3 = -0.04$ to 0.04 for a specific value of $a_4 \approx 0.24$. This indicates the possibility of multiple fission pathways involving symmetric ($a_3 = 0$) and asymmetric fission ($a_3 \neq 0$) modes.

Following the macroscopic approach, we advance to the microscopic description of the nucleus. In this framework, single-particle energy levels are determined by diagonalizing the Yukawa-folded mean-field Hamiltonian within a deformed harmonic oscillator basis. The nuclear shape is characterized using the Chebyshev shape parametrization, and calculations are performed for the nucleus ^{227}Pa at a specific deformation. Fig. 7 displays the single-particle energy levels for both protons and neutrons in ^{227}Pa , computed using three distinct shape parametrizations such as Chebyshev, Funny-Hills, and TKS. The deformation parameters are selected to yield identical nuclear shapes, with the following values for chebyshev $a_2 = -0.2475, a_3 = 0, a_4 = 0$ and $\eta = -0.15$; for Funny-Hills, $c = 2.020, h = -0.255, \alpha = 0.0$, and $\eta = -0.15$; and TKS, $\alpha_2 = -0.33, \alpha_3 = 0, \alpha_4 = 0$, and $\eta = -0.15$. The equivalence of these shapes is ensured through a transformation relation derived among the parametrizations from Eqs. 19, 20. The close agreement among the single-particle energy levels obtained from these three parametrizations at the specified deformation validates the robustness of our transformation relation and confirms the applicability of the Chebyshev

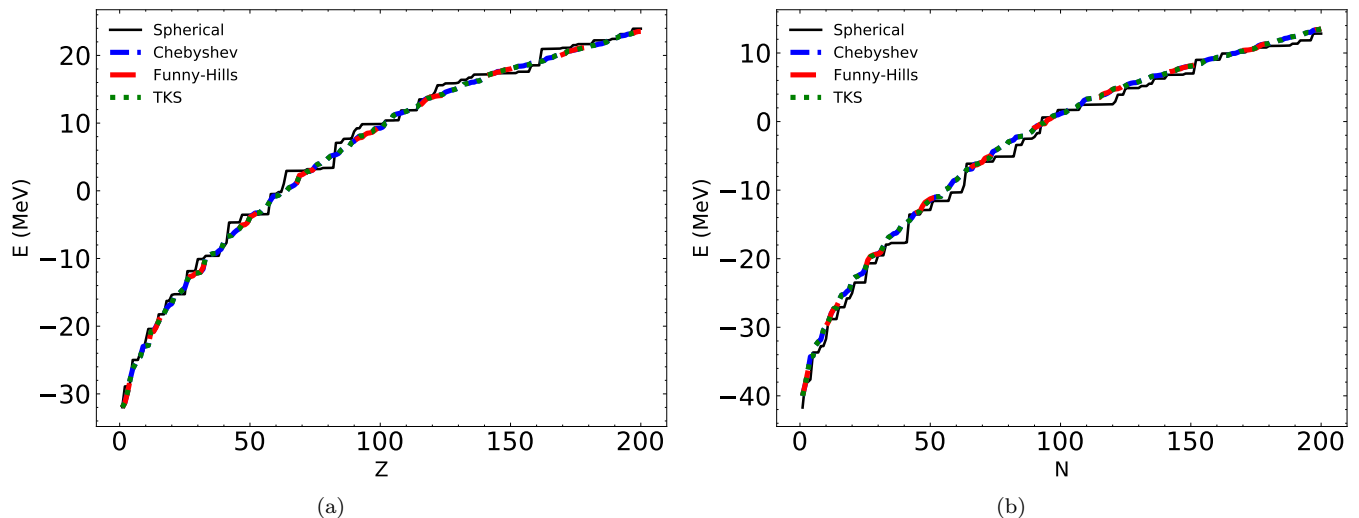


FIG. 7. Single-particle energy levels for (a) protons and (b) neutrons in the nucleus ^{227}Pa , calculated using different nuclear shape parametrizations: Chebyshev, Funny Hills, TKS. Results for the spherical shape, obtained using the Chebyshev parametrization, are also included for comparison.

shape parametrization for microscopic calculations.

IV. CONCLUSION

In this study, we have implemented a novel and effective Chebyshev shape parametrization approach to analyze the geometry of atomic nuclei and the energy landscape of nuclear systems within both macroscopic and microscopic frameworks. The deformation parameters derived through volume conservation and center-of-mass constraints have proven essential in describing various structural features of nuclei. In particular, we have elucidated the interconnected roles of a_2 and a_4 in governing nuclear elongation and neck formation, respectively, while a_3 captures asymmetry and η accounts for non-axiality. Our results demonstrate that the Chebyshev shape parametrization provides a more consistent formalism by offering transformation equations that connect it seamlessly with other widely used shape parametrizations. Through the deformation-dependent macroscopic energy coefficients, within the framework of LSD model, we have examined the potential energy surface and explored large amplitude phenomena. Specifically, the PES cross-section of ^{227}Pa was analyzed to investigate fission pathways and potential shape transitions under various deformations. Advancing to a microscopic description, we have computed single-particle energy levels by diag-

onalizing the Yukawa-folded mean-field Hamiltonian in a deformed harmonic oscillator basis, with the nuclear shape described by the Chebyshev parametrization. The results of selected deformations highlight the descriptive power of this approach in characterizing shell structures. As a future direction, we intend to enhance the potential energy calculations by incorporating shell and pairing corrections within a macroscopic-microscopic framework. This extension will further refine our understanding of nuclear structure and fission dynamics, emphasizing the intricate interplay among deformation parameters and their role in nuclear stability.

ACKNOWLEDGMENTS

K. Jyothish and M. S. Suryan Sivadas acknowledge the financial support provided by the Council of Scientific and Industrial Research (CSIR), India via grant numbers 09/239(0556)/2020-EMR-1 and 09/0239(11911)/2021-EMR-1 respectively. A. K. Rhine Kumar acknowledges the financial support provided by the Department of Science and Technology (DST), India, (DST/INSPIRE/04/2016/002545) via the DST-INSPIRE Faculty award. This work is also supported by the Science and Engineering Research Board (SERB), India, under Grant Code: CRG/2023/004323.

-
- [1] N. Schunck and D. Regnier, *Prog. Part. Nucl. Phys.* **125**, 103963 (2022).
 [2] N. Bohr and J. A. Wheeler, *Phys. Rev.* **56**, 426 (1939).

- [3] H. Krappe and K. Pomorski, *Theory of Nuclear Fission*, Vol. 843 of *Lecture Notes in Physics* (Springer, Berlin, 2012).

- [4] K. Mazurek *et al.*, Phys. Rev. C **84**, 014610 (2011).
- [5] F. A. Ivanyuk and K. Pomorski, Phys. Rev. C **79**, 054327 (2009).
- [6] W. D. Myers and W. J. Swiatecki, Nucl. Phys. **81**, 1 (1966).
- [7] P. Moller, J. Nix, W. Myers, and W. Swiatecki, At. Data Nucl. Data Tables **59**, 185 (1995).
- [8] R. W. Hasse and W. D. Myers, *Geometrical Relationships of Macroscopic Nuclear Physics* (Springer-Verlag, Berlin, 1988).
- [9] F. A. Ivanyuk, S. Chiba, and Y. Aritomo, Phys. Rev. C **90**, 054607 (2014).
- [10] L. Rayleigh, Proc. R. Soc. Lond. **29**, 71 (1879).
- [11] V. Pashkevich, Nucl. Phys. A **169**, 275 (1971).
- [12] V. Pashkevich and A. Rusanov, Nucl. Phys. A **810**, 77 (2008).
- [13] J. Rayford Nix, Nucl. Phys. A **130**, 241 .
- [14] P. Möller, D. G. Madland, A. J. Sierk, and A. Iwamoto, Nature **409**, 785 (2001).
- [15] M. Brack *et al.*, Rev. Mod. Phys. **44**, 320 (1972).
- [16] K. Mazurek *et al.*, Phys. Rev. C **88**, 054614 (2013).
- [17] K. Mazurek, P. N. Nadtochy, E. G. Ryabov, and G. D. Adeev, Eur. Phys. J. A **53**, 144 (2017).
- [18] K. Pomorski and J. Bartel, Int. J. Mod. Phys. E **15**, 417 (2006).
- [19] S. Trentalange, S. E. Koonin, and A. J. Sierk, Phys. Rev. C **22**, 1159 (1980).
- [20] C. Schmitt, K. Pomorski, B. Nerlo-Pomorska, and J. Bartel, Phys. Rev. C **95**, 034612 (2017).
- [21] G. Lalazissis, S. Raman, and P. Ring, Atom. Data Nucl. Data Tables **71**, 1 (1999).
- [22] M. Bender, P.-H. Heenen, and P.-G. Reinhard, Rev. Mod. Phys. **75**, 121 (2003).
- [23] S. Goriely, N. Chamel, and J. M. Pearson, Phys. Rev. Lett. **102**, 152503 (2009).
- [24] S. Goriely *et al.*, Phys. Rev. C **66**, 024326 (2002).
- [25] S. Goriely, S. Hilaire, M. Girod, and S. Péru, Phys. Rev. Lett. **102**, 242501 (2009).
- [26] J. Meng *et al.*, Prog. Part. Nucl. Phys. **57**, 470 (2006).
- [27] G. Gamow, Proc. R. Soc. Lond. A **126**, 632 (1930).
- [28] C. F. v. Weizsäcker, Zeitschrift für Physik **96**, 431 (1935).
- [29] H. A. Bethe and R. F. Bacher, Rev. Mod. Phys. **8**, 82 (1936).
- [30] P. Möller, W. Myers, W. Swiatecki, and J. Treiner, At. Data Nucl. Data Tables **39**, 225 (1988).
- [31] K. Pomorski and J. Dudek, Phys. Rev. C **67**, 044316 (2003).
- [32] V. Strutinsky, Nucl. Phys. A **95**, 420 (1967).
- [33] V. Strutinsky, Nucl. Phys. A **122**, 1 (1968).
- [34] P. Möller *et al.*, Phys. Rev. Lett. **103**, 212501 (2009).
- [35] W. Myers and W. Swiatecki, Nucl. Phys. A **601**, 141 (1996).
- [36] W. Myers and W. Swiatecki, Ann. Phys. **84**, 186 (1974).
- [37] W. D. Myers, At. Data Nucl. Data Tables **17**, 411 (1976).
- [38] K. Heyde and J. L. Wood, Rev. Mod. Phys. **83**, 1467 (2011).
- [39] J. Dudek, K. Pomorski, N. Schunck, and N. Dubray, Eur. Phys. J. A **20**, 15 (2003).
- [40] K. Pomorski *et al.*, Eur. Phys. J. A **58**, 77 (2022).
- [41] A. K. Rhine Kumar, P. Arumugam, N. D. Dang, and I. Mazumdar, Phys. Rev. C **96**, 024322 (2017).
- [42] J. Mason and D. Handscomb, *Chebyshev Polynomials*, 1st ed. (Chapman and Hall/CRC, New York, 2002).
- [43] J. P. Boyd, *Chebyshev and Fourier Spectral Methods*, 2nd ed. (Dover Publications, Mineola, New York, 2001).
- [44] D. Gottlieb and C.-W. Shu, SIAM Review **39**, 644 (1997).
- [45] L. N. Trefethen, *Approximation Theory and Approximation Practice* (Society for Industrial and Applied Mathematics (SIAM), Philadelphia, PA, 2013).
- [46] T. J. Rivlin, *Chebyshev polynomials* (Dover Publications, Mineola, New York, 2020).
- [47] C. W. Clenshaw, Math. Proc. Camb. Philos. Soc. **53**, 134–149 (1957).
- [48] P. Nadtochy *et al.*, Comput. Phys. Commun. **258**, 107605 (2021).
- [49] J. Bartel, B. Nerlo-Pomorska, K. Pomorski, and A. Dobrowolski, Comput. Phys. Commun. **241**, 139 (2019).
- [50] K. Pomorski, B. Nerlo-Pomorska, and J. Bartel, Physica Scripta **92**, 064006 (2017).
- [51] B. Nerlo-Pomorska, K. Pomorski, C. Schmitt, and J. Bartel, Physica Scripta **90**, 114010 (2015).
- [52] A. Dobrowolski, K. Pomorski, and J. Bartel, Comput. Phys. Commun. **199**, 118 (2016).
- [53] N. Schunck and L. Robledo, Rep. Prog. Phys. **79**, 116301 (2016).
- [54] P. Jachimowicz, M. Kowal, and J. Skalski, Phys. Rev. C **87**, 044308 (2013).
- [55] J. R. Nix, Ann. Phys. **41**, 52 (1967).
- [56] D. L. Hill and J. A. Wheeler, Phys. Rev. **89**, 1102 (1953).
- [57] A. Dobrowolski, K. Pomorski, and J. Bartel, Phys. Rev. C **75**, 024613 (2007).
- [58] P. V. Kostyukov *et al.*, Chin. Phys. C **45**, 124108 (2021).
- [59] L.-L. Liu *et al.*, Phys. Rev. C **99**, 044614 (2019).
- [60] A. Dobrowolski *et al.*, Comput. Phys. Commun. **199**, 0010-4655 (2016).
- [61] P. V. Kostyukov and A. Dobrowolski, Phys. Rev. C **108**, 024605 (2023).
- [62] K. Pomorski *et al.*, Phys. Rev. C **107**, 054616 (2023).
- [63] S. R. Reddy *et al.*, Phys. Rev. C **110**, 014622 (2024).
- [64] N. Saneesh *et al.*, Phys. Rev. C **108**, 034609 (2023).